Scientia Iranica, Vol. 10, No. 2, pp 211–219

SCIENTIA
IRANICA

Numerical Prediction and Measurement of Carbon Black Through Turbulent Combustion and Decomposition of Natural Gas

M. Moghiman[1]

In this paper, the measurements and evolution of a 3-D numerical solution procedure are described for prediction and valuation the production of carbon black in the course of turbulent incomplete combustion and thermal decomposition of natural gas in a gas carbon black furnace. A particle collection system is used to measure the carbon black concentrations in the furnace. In the numerical technique, a combination of a two-step soot model and a chemical reaction formulation relates the production of the carbon black to the incomplete combustion and pyrolysis of natural gas as the parent fuel. The chemical reaction model, which involves solid carbon and other precursor species for formation of carbon black, based on an assumed Probability Density Function (PDF) is parameterized by the mean and variance of the mixture fraction and β-PDF shape. The effect of feedstock flow rate, equivalence ratio and radiation on carbon black furnace parameters are investigated. The comparison between numerical predictions and experimental measurements show good agreement. The results show that for relatively low feedstock flow rates, most feedstock hydrocarbon burns to CO while, for higher feedstock flow rates, the decomposition of feedstock and formation of solid carbon is the dominant process and has an important role in the production of carbon black. The results also show that radiation has a major influence on the precombustor where most soot combustion takes place, causing a reduction of about 10% in the precombustor temperature.

INTRODUCTION

Carbon black has been widely used in industry, especially in rubber and plastic production. The gas furnace process for the production of carbon black was applied at the beginning of this century, but was later replaced by the cheaper oil furnace process. A possible new application - the production of carbon black from associated oilfield gas - raises new interest in this process. Flaring or venting of natural gas which is a very wasteful practice and causes environmental pollution, can be avoided by using the gas furnace black process. In comparison with liquid fuels, the gaseous fuels do not lose the heat of evaporation and have the advantage of mixing rapidly with hot gases.

In practical carbon black furnaces, the two main processes of carbon black production are incomplete combustion and thermal decomposition of feedstock hydrocarbon fuels [1]. In the precombustor of the furnace (Figure 1), the turbulent lean combustion of fuel raises gas temperature in the mixing zone and reactor, where feedstock hydrocarbon rapidly meets and mixes with the stream of hot gases. Turbulent rich combustion and thermal decomposition of feedstock produces carbon black and other precursor species for the formation of carbon black. Almost all the soot formed in the precombustor diffusion flame is consumed through oxidation by the precombustor excess air and other oxygenated species. Soot oxidation which is the primary method by which soot is normally consumed is accompanied by radiation which has considerable influence on the heat transfer [2].

The production of carbon black particles involves a complex series of chemical and physical processes which control both the conversion of fuel carbon to carbonaceous particles and growth or, probably, com-

1. *Department of Mechanical Engineering, University of Ferdowsi, Mashad, I.R. Iran.*

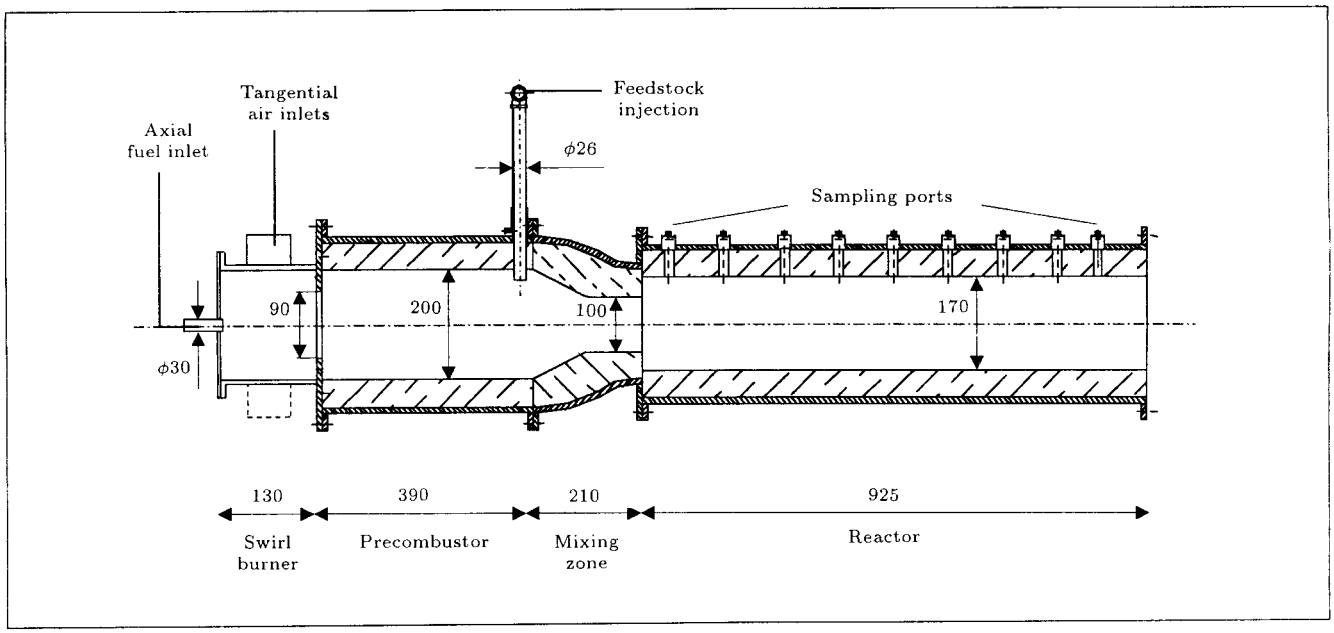

Figure 1. Carbon black gas furnace.

bustion of some of these particles. A comprehensive model of carbon black prediction must include all of these processes. Although many useful attempts at soot prediction modeling have been made, no generally applicable model considering all aspects of turbulent combustion and decomposition processes has yet been devised [1,3,4]. Despite the highly turbulent nature of most practical combustion applications, due to the difficulties of solving an excessively large number of partial differential equations, studies of numerical soot predictions have been typically limited by the use of one- or two-dimensional laminar combustion phenomena and simplified or quasi-global models [5,6]. Recent advances in the size and speed of digital computers have allowed the possibility of employing sophisticated CFD techniques and comprehensive mathematical models to predict detailed turbulent reacting flows and combustion properties in combustion systems with complex physical geometry.

The purpose of this paper is the evaluation of carbon black formation through experimental measurements and modification and utilization of a 3-D numerical technique, which predicts detailed turbulent flame structure and relates carbon black formation to both specific pyrolysis species and soot formation through incomplete combustion of natural gas. Based on the modern oil furnace process [1], an axial flow carbon black gas furnace (max. performance 5-10 kg carbon black per hr) has been designed and manufactured employing the same principles but using natural gas as feedstock (Figure 1). The design of the furnace allows the adjustment of all relevant process parameters such as equivalence ratio, feedstock flow rate and air feedstock ratio.

EXPERIMENTAL CARBON BLACK FURNACE AND MEASUREMENTS

The carbon black furnace used in this investigation, is a simplified generic small-scale axial flow gas furnace. It has been designed and manufactured based on the modern oil furnace process but using natural gas as feedstock hydrocarbon (max. performance 5-10 kg carbon black per hour). The basic geometry of the carbon black furnace is shown in Figure 1, consisting of a precombustor, a mixing zone and a reactor. In the precombustor, the axially injected natural gas fuel burns with the process air, which is introduced through two tangential inlets. The highly swirling hot gases meet the feedstock natural gas fuel, which is injected radially into the precombustor in the vicinity of the mixing zone. The abrupt enlargement in diameter at the exit of the choke encourages the mixing of feedstock fuel with the hot gases. The design of the furnace allows the adjustment of all relevant process parameters such as air/fuel ratio, air/feedstock ratio and reactant preheat temperatures. The carbon black concentrations in the furnace were determined using a particle collection system. This involved isokinetic sampling from the flames, followed by measurement of the gas and carbon black volumes in the samples. Tests were carried out with a sampling ID 6 mm and a suction rate of 2.5 l/min, leading to near isokinetic conditions (sampling: 1.5 m/s; flow: $\approx$ 2 m/s). The 90°-bent nozzle design used in this study shows lower particle deposition losses within the nozzle [7]. A fiber filter was installed in the probe tube and its weight was measured before and after sampling, using an analytical balance (Mettler AE 50-S, Metter Instru-

ments Ltd, High Wycombe, UK) with an accuracy of ± 0.1 mg. The filters were dried for 1 hour at 125°C before each weighing. Type R thermocouples, which were used in this work for accuracy, measure absolute temperatures within a tolerance of ± 50°C and relative temperatures within ± 5°C. As the carbon deposition on the bead of thermocouples can have a significant impact on the temperature measurements, measurements were carried out with a clean bead. Experimental measurements were carried out for precombustor fuel flow rate of 0.135 m^3/min and different feedstock flow rates. Air flow rate was 1.4 m^3/min at 400°C.

CHEMICAL REACTION MODELING

The feedstock furnace process is based on the incomplete combustion of methane:

$$2CH_4 + 2O_2 \rightarrow CO_2 + 2H_2 + 2H_2O + C_S, \quad \text{(Reaction 1)}$$

and thermal decomposition of methane [8]:

$$CH_4 + \text{Energy} \rightarrow C_S + 2H_2. \quad \text{(Reaction 2)}$$

Such an endothermic decomposition is at relatively high temperatures. The main problem in the prediction of carbon black formation is the modeling of both fuel combustion and decomposition, simultaneously. The mixture fraction / PDF method is used to model the turbulent chemical reactions occurring in the diffusion, combustion and thermal decomposition of natural gas in the carbon black furnace. This method, which assumes that the chemistry is fast enough for a chemical equilibrium to always exist at molecular level, enables the handling of large numbers of reacting species, including intermediate species. In non-adiabatic systems, where change in enthalpy, due to heat transfer, affects the mixture state, the instantaneous thermochemical state of the mixture, resulting from the equilibrium chemistry model, is related to a strictly conserved scalar quantity known as the mixture fraction, f, and the instantaneous enthalpy, $H^*, \phi_i = \phi_i(f, H^*)$. The effects of turbulence on the thermochemical state are accounted for with the help of a probability density function (PDF):

$$\overline{\phi_i} = \int_0^1 \phi_i(f, \overline{H^*}) p(f) df. \quad (1)$$

As in carbon black furnaces, the heat transfer from walls is not high. For simplicity, it has been assumed that heat losses do not, significantly, impact on the turbulent enthalpy fluctuations.

In this study, the β-probability density function used by Jones and McGuirk [9] is used to relate the time-averaged values of individual species mass fractions, the temperature and the fluid density of the mixture to instantaneous mixture fraction fluctuations. The β-probability density function, in terms of the mean mixture fraction $\overline{f}$ and its variance $\overline{f'^2}$, can be written as:

$$P(f) = \frac{f^{\alpha-1}(1-f)^{\beta-1}}{\int_0^1 f^{\alpha-1}(1-f)^{\beta-1} df}, \quad 0 \prec f \prec 1, \quad (2)$$

where:

$$\alpha = \overline{f}\left[\frac{\overline{f}(1-\overline{f})}{\overline{f'^2}} - 1\right],$$

$$\beta = (1-\overline{f})\left[\frac{\overline{f}(1-\overline{f})}{\overline{f'^2}} - 1\right]. \quad (3)$$

Using the unweighted averaging [10], the values of the two parameters $\overline{f}$ and $\overline{f'^2}$ at each point in the flow domain are computed through the solution of the following conservation equations [11]:

$$\frac{\partial}{\partial x_i}\left(\rho u_i \overline{f}\right) = \frac{\partial}{\partial x_i}\left(\frac{\mu_t}{\sigma_t}\frac{\partial \overline{f}}{\partial x_i}\right), \quad (4)$$

$$\frac{\partial}{\partial x_i}\left(\rho u_i \overline{f'^2}\right) = \frac{\partial}{\partial x_i}\left(\frac{\mu_t}{\sigma_t}\frac{\partial \overline{f'^2}}{\partial x_i}\right) + C_g \mu_t \left(\frac{\partial \overline{f}}{\partial x_i}\right)^2 - C_d \rho \frac{\varepsilon}{k}\overline{f'^2}, \quad (5)$$

where the constants $\sigma_t, C_g(= 2/\sigma_t)$ and C_d take the values 0.7, 2.86 and 2.0, respectively [10]. The transport equation, which calculates the distribution of the instantaneous enthalpy, is as follows:

$$\frac{\partial}{\partial x_i}(\rho u_i \overline{H^*}) = \frac{\partial}{\partial x_i}\left(\frac{k_t}{c_p}\frac{\partial \overline{H^*}}{\partial x_i}\right) + \tau_{ik}\frac{\partial u_i}{\partial x_k} + S_h, \quad (6)$$

where k_t is turbulent thermal conductivity and S_h includes the heat of the chemical reaction and radiation. The instantaneous enthalpy is defined as:

$$H^* = \sum_j m_j H_j = \sum_j m_j \left[\int_{T_{\text{ref},j}}^{T} c_{p,j} dT + h_j^\circ(T_{\text{ref},j})\right], \quad (7)$$

where m_j is the mass fraction of species j and $h_j^\circ(T_{\text{ref},j})$ is the formation enthalpy of species j at the reference temperature $T_{\text{ref},j}$.

SOOT FORMATION / OXIDATION MODEL

In this study, the two-step empirical model of Tenser et al. [12] is used to predict the formation / oxidation of soot. This model takes into account the particle inception, surface growth and oxidation of soot particles in diffusion flames. Considering decomposition processes

due to high temperatures, Tenser et al. constructed the kinetics of the process based on a chain-type radical process. They used the idea of the formation of some active radical particles, named nuclei, from which soot particles would later grow. In this model, the rate of nuclei formation, $R_{N,f}$ depends on a global, branched-chain process, described by:

$$R_{N,f} = n_0 + (f - g)n_N - g_0 n_S n_N, \tag{8}$$

where $R_{N,f}$ is the rate of nuclei formation and n_0 is the kinetic rate which is a temperature dependent rate of spontaneous generation of nuclei and obtained as: $n_0 = a_0 c_F \exp(-E/RT)$. Here, a_0 is the pre-exponential rate (particles/kg-s), c_F is the fuel concentration (kg/m^3), f and g are branching and termination coefficients, g_0 is the rate of loss of nuclei due to collisions with soot particles (m^3/particles-s), and n_S and n_N are the concentration of soot and radical nuclei particles (particles/m^3), respectively.

Tesner et al. proposed a rate equation for the particle forming step and evaluated the coefficients in their equations with experimental data, viz.

$$\frac{dn_S}{dt} = (a - bn_S)n_N, \tag{9}$$

where a and b are the constant parameters. The coefficient values of the Tesner model are as [12,13]: $a = 10^5(1/s), (f - g) = 10^2(1/s), b = 8 \times 10^{-8}$ (m^3/particles), $a_0 = 2.32 \times 10^{17}$ (particle/kg-s), $E/R = 90 \times 10^4$ K. Magnussen constant = 4.

The distribution of the mass fraction of radical nuclei is obtained through the solution of the following transport equation:

$$\frac{\partial}{\partial t}(\rho m_N) + \frac{\partial}{\partial x_i}(\rho u_i m_N) = \frac{\partial}{\partial x_i}\left(\frac{\mu_t}{\sigma_N}\frac{\partial m_N}{\partial x_i}\right) + R_N, \tag{10}$$

where $m_N = n_N/\rho$ (particles/kg), σ_N is the turbulent Prandtl number for nuclei transport and R_N is the net rate of nuclei generation (particles/m^3-s), which involves a balance between formation and combustion. The rate of nuclei combustion is assumed to be proportional to the rate of soot combustion:

$$R_{N,c} = R_{S,c}\frac{n_N}{n_S}, \tag{11}$$

where $R_{S,c}$ is obtained from Equation 13.

The rate of soot formation, $R_{S,f}$, depends on the concentration of radical nuclei:

$$R_{S,f} = m_p(\alpha - \beta n_S)n_N, \tag{12}$$

where:

m_p	=	mean mass of soot particles (kg/particle)
α	=	empirical constant (1/s)
β	=	empirical constant (m^3/particles-s)

The generalized formulation of Magnussen and Hjertager [14] is used to determine the rate of soot combustion:

$$R_{S,c} = \left[\left|Am_S\rho\frac{\varepsilon}{k}, A\frac{m_0}{S_S}\frac{m_S S_S}{m_S S_S + m_F S_F}\rho\frac{\varepsilon}{k}\right|\right] \tag{13}$$

where:

A	= constant in the Magnussen model
m_S, m_0, m_F	= mass fraction of soot, oxidiser and fuel
S_S, S_F	= mass stoichiometries for soot and fuel combustion
k	= kinetic energy of turbulence
ε	= dissipation rate of turbulence energy

the operator $[|\cdots|]$ takes the smaller of the expressions in the brackets.

The solution of a transport equation describes the distribution of soot concentration:

$$\frac{\partial}{\partial t}(\rho m_S) + \frac{\partial}{\partial x_i}(\rho u_i m_S) = \frac{\partial}{\partial x_i}\left(\frac{\mu_t}{\sigma_S}\frac{\partial m_S}{\partial x_i}\right) + R_S, \tag{14}$$

where σ_S is the turbulent Prandtl number for soot transport and R_S is the net rate of soot generation, which is the balance of soot formation and soot combustion:

$$R_S = R_{S,f} - R_{S,c}. \tag{15}$$

RADIATION MODEL

The radiative heat transfer in the absorbing, emitting and scattering medium is calculated by the Discrete Ordinates (DO) radiation model [15]. The radiative transfer equation in the direction **s** and in terms of the spatial coordinates, x_I, is as follows:

$$\frac{d(I_{s_i})}{dx_i} + (a_g + \sigma_s)I(r,s) = a_g\frac{\sigma T^4}{\pi} + \frac{\sigma_s}{4\pi}\int_0^{4\pi} I(r,s')d\Omega', \tag{16}$$

where:

I	= total radiation intensity
s_I	= components of **s**
a_g	= absorption coefficient of gas
σ_s	= scattering coefficient
σ	= Stefan-Boltzmann constant (5.672×10^{-8} W/m^{2}K^4)
r	= position vector
T	= local temperature
s	= direction vector
s'	= scattering direction vector
Ω'	= solid angle

The discrete ordinates model solves the radiative transfer Equation 16 for a finite number of discrete solid

angles, each associated with a vector direction, **s**, fixed in the global Cartesian system (x, y, z). The weighted-sum-of-gray-gases model [16] is used to determine the variable absorption coefficient. When $s \leq 10^{-4}$ m, the equation for absorption coefficient, a_g, is as:

$$a_g = \sum_{i=0}^{I} a_{E,i} k_i P, \tag{17}$$

where $a_{E,I}$ are the emissivity weighting factors for the Ith fictitious gray gas, k_I is the absorption of the ith gray gas and p is the sum of partial pressures of all absorbing gases. For $a_{E,I}$ and k_I, values obtained from [16] were used. When $s \geq 10^{-4}$ m, the absorption coefficient is calculated from:

$$a_g = -\ln(1-\varepsilon)/s, \tag{18}$$

where s is the path length, which is determined by the characteristic cell size and the emissivity, ε, is computed using the following equation:

$$\varepsilon = \sum_{i=0}^{I} a_{\varepsilon,i}(T)[1 - \exp(-k_i P s)]. \tag{19}$$

The effect of carbon black concentration on the radiation absorption coefficient is included, using an effective absorption coefficient for carbon black. The absorption coefficient of a mixture of carbon black and an absorbing radiating gas is calculated as the sum of the absorption coefficient of pure gas and pure carbon black:

$$a_{cb+g} = a_g + a_{cb}, \tag{20}$$

and

$$a_{cb} = b_1 c_m [1 + b_T (T - 2000)], \tag{21}$$

where c_m is the carbonblack concentration in kg/m^3 and the coefficients b_1 and b_T are obtained from [17]: $b_1 = 1232.4$ m^3/kg and $b_T \approx 4.8 \times 10^{-4} 1/K$.

Although most of the gases present in the combustion systems, such as carbon dioxide and water vapor, are strong absorbers and emitters, they do not scatter radiation significantly [18]. Scattering was assumed to be isotropic and the scattering coefficient was set to 1×10^{-5} [18].

NUMERICAL SOLUTION PROCEDURE

Fluent CFD software [19], which allows one to model furnaces with complex geometry and solution- adaptive grid-refinement, has been applied in this study to solve the 3D problem. Gambit and TGrid preprocessors were used for the fully three-dimensional geometry creation and unstructured grid generation, respectively. The 3D volume grid is represented in Figure 2. The

Figure 2. Three-dimensional grid (enlarged cell size for presentation purpose).

domain was discretized into a grid of 15713 nodes and 74170 tetrahedral cells. The conservation equations of mass, momentum, Reynolds stresses, dissipation rate, mixture fraction and its variance and concentration of soot and nuclei were solved by applying a conventional finite-volume treatment, using a second-order upwind scheme for discretisation of the convective terms of transport equations. A Reynolds Stress Model of turbulence (RSM) was used instead of the more usual $k - \varepsilon$ model, since clear evidence exists that prediction of anisotropic, highly swirling and recirculating flow is otherwise unsatisfactory [20]. Abandoning the isotropic eddy-viscosity hypothesis, the RSM closes the Reynolds-averaged Navier-Stokes equations by solving six differential transport equations for Reynolds stresses, together with an equation for the dissipation rate of turbulence kinetic energy [21]. The conventional wall-function approach was used in the near-wall region [22]. At the inlet boundary, conditions were specified once and did not need updating during the course of the solution procedure. At the outlet boundary, zero gradient conditions were applied. A fixed temperature condition was applied at the wall of the furnace. A grid dependence study was conducted to arrive at the appropriate size of the grid to combine accuracy and efficiency. The number of grid points was varied from 13517, 15713 to 170411 for a typical set of operating conditions. It was observed that the field quantities varied less than 1% after the number of grid points was increased beyond 15713. For the radiation model, emissivity coefficients at the flow inlets and outlets were taken to be 1.0 (black body absorption). Wall emissivity was set to be 0.6, a typical value for gas combustion.

RESULTS

The measurements and numerical calculations were carried out for a total precombustor inlet airflow rate of 23×10^{-3} m^3/s, at a temperature of 673 K and normal atmospheric pressure of 1 bar. The equivalence ratio used for the precombustor was 0.941.

Figure 3 shows the calculated distributions for CH_4, temperature, nuclei, soot and solid carbon, which have been obtained for 3.2×10^{-3} kg/s of feedstock flow rate. Of particular importance are Figures 3c to 3e, showing the formation of carbon nuclei from the entering feedstock methane jet (Figure 3c), soot production from the interaction and breakdown of the methane

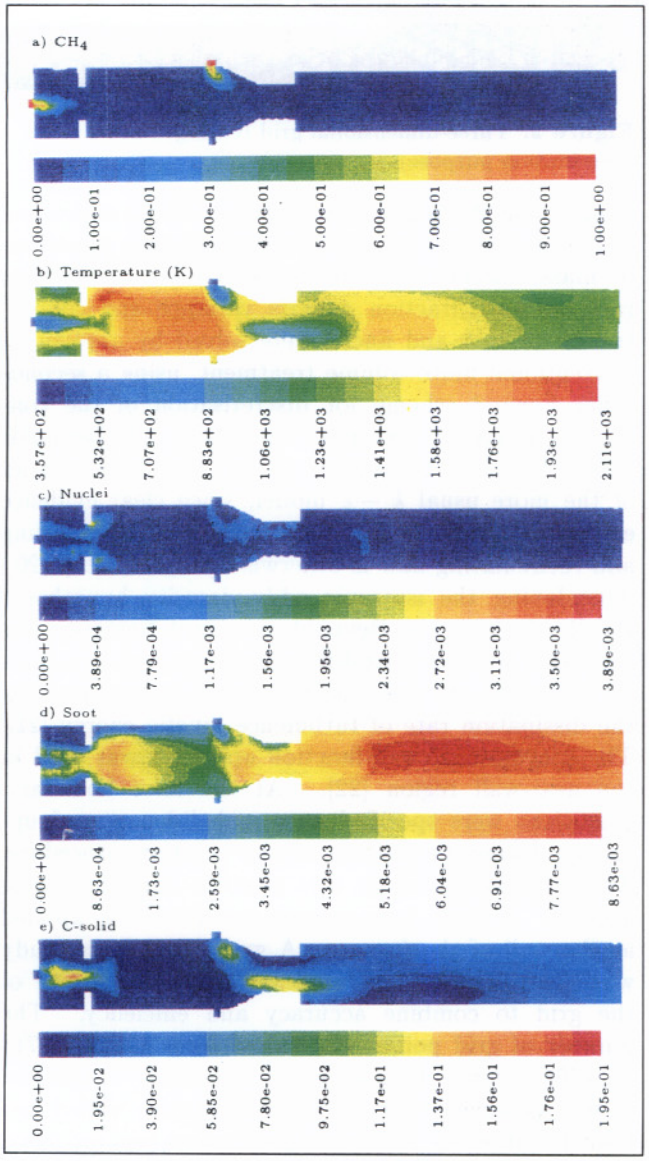

Figure 3. Contours of species mass fractions and temperature (K).

jet with hot combustion products and the production of solid carbon again from the entering methane jet interacting with hot surroundings. Clearly, the use of more inlets for the feedstock methane injection would have improved flow and aerochemistry symmetry and, undoubtedly production of carbon black. Experimental conditions precluded this.

Figure 4 shows the calculated effect of feedstock flow rate on soot, solid carbon and carbon black (the summation of soot and solid carbon) at the outlet of the furnace. It can be seen that for lower values of feedstock, as the reactor temperature values are high (see Figure 7), the values of C(s) are low because most feedstock burns to CO (see Figure 9) and some of it forms soot. For higher flow rates of feedstock (which is a cold gas), higher values of C(s) are formed and,

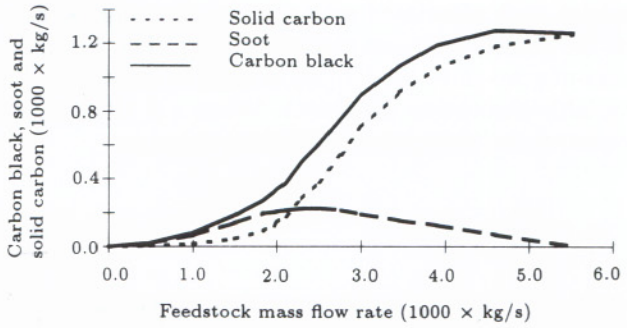

Figure 4. Effect of feedstock flow rate on calculated solid carbon and carbon black formation.

due to reduction of temperature, the formation of CO and soot decreases (the soot model strongly depends on temperature).

Figure 5 shows the influence of furnace equivalence ratio on measured carbon black parameters, namely, carbon black production (defined as kg carbon black/kg process air), carbon black yield (kg carbon black/kg feedstock), carbon black total yield (kg feedstock/kg precombustor fuel + kg feedstock) and carbon black mass fraction (kg carbon black/kg total flow). The equivalence ratio of the furnace is increased by an increase in the feedstock hydrocarbon at a constant air and fuel process. The increase in equivalence ratio results in an increased carbon black production, yield, total yield and mass fraction up to their respective maxima. The maxima of the two yields occur at the same equivalence ratio and differ from the equivalence ratio at which the maxima of carbon black production and mass fraction occur.

Figure 6 shows the results of a variation of air/feedstock ratio on the measured production parameters of carbon black. As the air flow rate is kept constant the variation in air/feedstock ratio is due to the variation in feedstock flow rate. It is seen that the maximum carbon black mass fraction is reached at a lower air/feedstock ratio than the maximum carbon black yield. This result and the trend of a variation of carbon black parameters in response

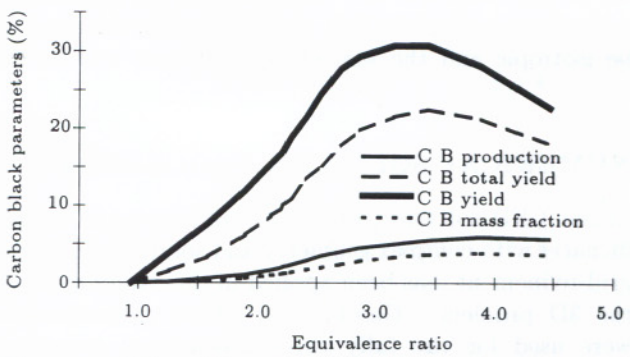

Figure 5. Effect of furnace equivalence ratio on measured carbon black parameters.

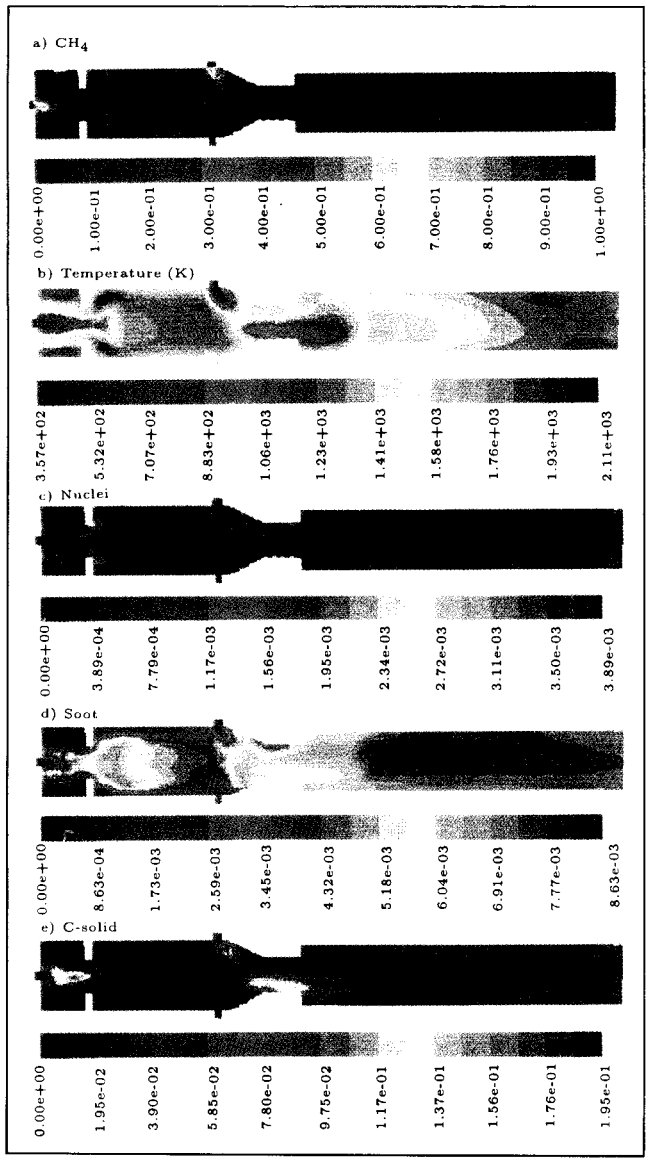

Figure 3. Contours of species mass fractions and temperature (K).

jet with hot combustion products and the production of solid carbon again from the entering methane jet interacting with hot surroundings. Clearly, the use of more inlets for the feedstock methane injection would have improved flow and aerochemistry symmetry and, undoubtedly production of carbon black. Experimental conditions precluded this.

Figure 4 shows the calculated effect of feedstock flow rate on soot, solid carbon and carbon black (the summation of soot and solid carbon) at the outlet of the furnace. It can be seen that for lower values of feedstock, as the reactor temperature values are high (see Figure 7), the values of C(s) are low because most feedstock burns to CO (see Figure 9) and some of it forms soot. For higher flow rates of feedstock (which is a cold gas), higher values of C(s) are formed and,

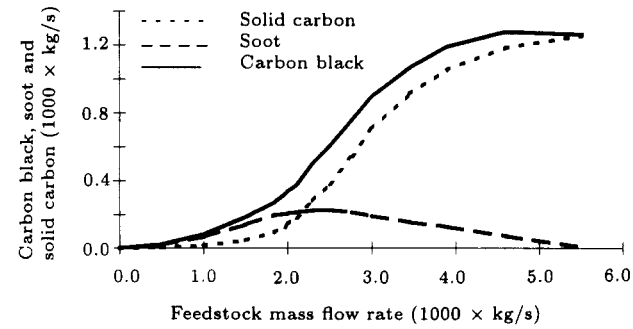

Figure 4. Effect of feedstock flow rate on calculated solid carbon and carbon black formation.

due to reduction of temperature, the formation of CO and soot decreases (the soot model strongly depends on temperature).

Figure 5 shows the influence of furnace equivalence ratio on measured carbon black parameters, namely, carbon black production (defined as kg carbon black/kg process air), carbon black yield (kg carbon black/kg feedstock), carbon black total yield (kg feedstock/kg precombustor fuel + kg feedstock) and carbon black mass fraction (kg carbon black/kg total flow). The equivalence ratio of the furnace is increased by an increase in the feedstock hydrocarbon at a constant air and fuel process. The increase in equivalence ratio results in an increased carbon black production, yield, total yield and mass fraction up to their respective maxima. The maxima of the two yields occur at the same equivalence ratio and differ from the equivalence ratio at which the maxima of carbon black production and mass fraction occur.

Figure 6 shows the results of a variation of air/feedstock ratio on the measured production parameters of carbon black. As the air flow rate is kept constant the variation in air/feedstock ratio is due to the variation in feedstock flow rate. It is seen that the maximum carbon black mass fraction is reached at a lower air/feedstock ratio than the maximum carbon black yield. This result and the trend of a variation of carbon black parameters in response

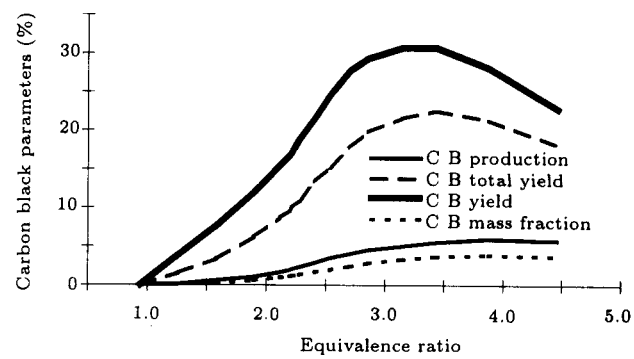

Figure 5. Effect of furnace equivalence ratio on measured carbon black parameters.

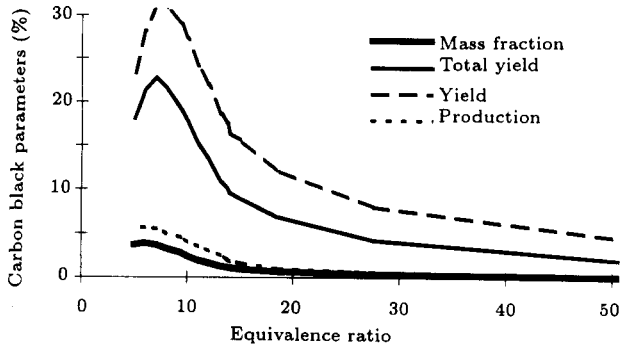

Figure 6. Effect air/feedstock ratio variation on measured carbon black parameters.

to the variation of air/feedstock ratio, are similar to the results obtained by Lockwood and Niekerk for oil carbon black furnaces [1].

Figure 7 presents the comparison between predicted and measured reactor average temperatures for various feedstock flow rates. The predicted results are shown for two conditions: With and without considering the radiation heat transfer. It can be seen that all results show that an increase in feedstock flow rate results in a decrease in reactor temperature. This occurs because heat is required for both heating up and decomposing the cold feedstock hydrocarbon. It is seen that for lower feedstock flow rates, the trend of a reduction in temperature is slow and this occurs because some feedstock burns to CO, using the amount of oxygen in the precombustor effluent (depending on the equivalence ratio) or by obtaining it from oxygenated species like CO_2 and OH (see Figure 11). The predicted results show that radiation has reduced the precombustor effluent temperature by about 10%. This occurs because considerable soot is burned in the precombustor (see Figure 3). The comparison between calculated and measured temperatures reveals that the numerical results show higher temperatures for the precombustor effluent gases than the experimental results. The experimental results show that the average temperature of precombustor effluent gases is about 2000°K, which seems about 10% lower than temperature levels used in the liquid fuelled carbon black furnaces. This can have an effect on carbon black production (see Figure 8).

Figure 8 shows the comparison between predicted and measured carbon black and hydrogen mass fractions for relatively low feedstock flow rates (as mentioned before, due to some limitation for the experimental tests, utilization of higher feedstock flow rate was impossible). It can be seen that the predicted mass fractions of H_2 are higher than the measured values. This occurs because of higher feedstock decomposition, due to a higher precombustor effluent gas temperature. The predicted carbon black mass fraction for very low feedstock flow rates is a little lower than measured values. This happens because, due to a higher calculated temperature, more carbon is burned to CO (see Figure 9). For higher feedstock flow rates, the predicted carbon black mass fraction is somewhat higher than the experimental measurements.

Figure 9 shows the comparison between predicted and measured CO and CH_4 mass fractions at the outlet of the furnace. The experimental results show that about 30% of feedstock hydrocarbon leaves the furnace without any chemical change. This can be reduced by

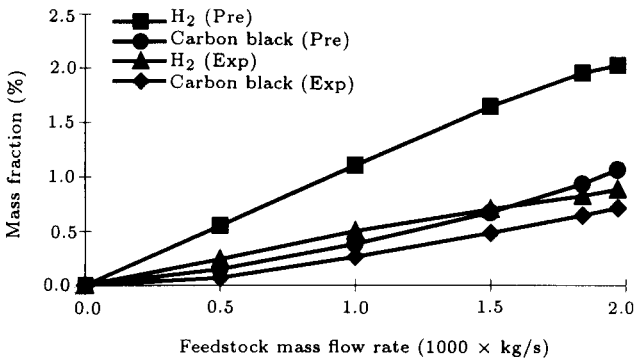

Figure 8. Computed and measured carbon black and hydrogen furnace output.

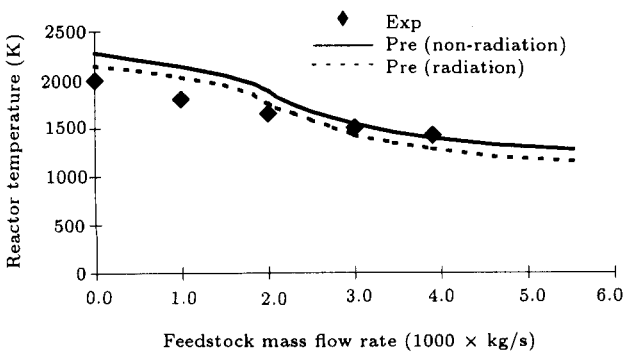

Figure 7. Effect of feedstock flow rate and radiation reactor temperature.

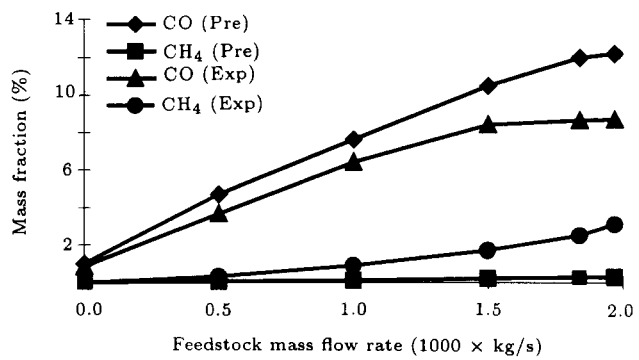

Figure 9. Computed and measured CO and CH_4 furnace output.

creating higher temperatures in the precombustor and probably improving the mixing process in the mixing zone. It can be seen that the numerical technique predicts lower mass fractions for CH_4 and higher values for CO at the outlet of the furnace.

Figure 10 shows the comparison between predicted and measured carbon black yield and total yield at the outlet of the furnace. It can be seen that the results of the two methods are very close, especially for lower feedstock flow rates. For higher feedstock mass flow rates, the prediction method shows higher carbon black production.

Figure 11 shows the predicted variations of CO, CO_2 and H_2 mass fractions for different values of feedstock flow rates at the outlet of the furnace. It is seen that for low values of the feedstock flow rate, the very hot precombustor effluent causes the feedstock to be burnt to CO (as mentioned above) using the oxygen in the precombustor effluent and, by reduction, CO_2. For higher flow rates of cold feedstock, the decomposition of natural gas reduces the reactor temperature and, consequently, reduces the production of CO and consumption of CO_2. The variation of H_2 mass fraction represents the variation of feedstock decomposition.

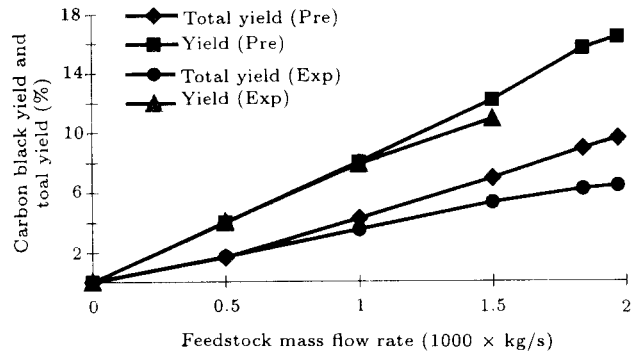

Figure 10. Computed and measured carbon black yield and total yield.

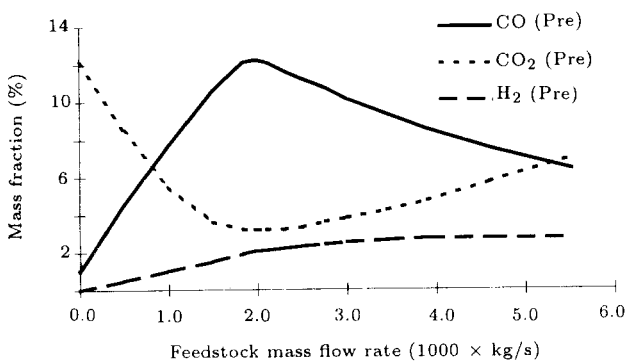

Figure 11. Effect of feedstock flow rate on calculated CO, CO_2 and H_2 mass fractions.

CONCLUSIONS

Comparison of experimentally measured parameters from a natural gas fuelled, swirl stabilized, carbon black reactor shows that a 3-D CFD technique, with a PDF combustion and a two-step empirical model for soot formation/oxidation, enables the main trends of carbon black formation in the reactor to be modeled. In detail, it is clear that improvements in the CFD code can be made in prediction of hydrogen formation across the whole load range. CO and CH_4 formation is best predicted at low feedstock mass flow rates. Deviation at high flow rates, possibly more species and a reaction in the chemical scheme could have improved these predictions.

The known limitation of this model is the use of equilibrium chemistry in the PDF model. However, the results indicate that over much of the reactor such an assumption is not too unreasonable, considering the fairly restrictive nature of the chemical model used.

An important conclusion, reinforcing that of other works in the field, is that the equivalence ratios at which carbon black production and carbon black yield occur differ. However, production of carbon black is obtained at lower air/feedstock ratios than those for highest yield. Clearly there is considerable scope for optimizing the process using the derived experimental results and the CFD code. For example, the use of more inlets for the feedstock would clearly improve symmetry and the production of carbon black. For this project, however, these were limited on the experimental rig.

REFERENCES

1. Lockwood, F.C. and Niekerk, J.E. VAN, "Parametric study of a carbon black oil furnace", *Combustion and Flame*, **103**, pp 76-90 (1995).
2. Kollmann, W., Kennedy, I.M., Metternich, M. and Chen, J.Y. "Application of a soot model to a turbulent ethylene diffusion flame", in *Soot Formation in Combustion*, H. Bockhorn, Ed., Springer-Verlag, pp 503-526 (1994).
3. Kennedy, I.M., Celement, Yam, Rapp Darrell C. and Santoro, R.J. "Modelling and measurements of soot and species in a laminar diffusion flame", *Combustion and Flame*, **107**, pp 368-382 (1996).
4. Hayashi, S., Furuhata, T., Aoki, H. and Miura, T. "Simulation of soot formation behaviour in carbon black furnace", *Proceedings of ICLASS*, pp 1106-1113, Seoul, Korea (1997).
5. Farmer, R., Edelman, R., and Wong, E., "Modelling soot emissions in combustion systems", *Particulate Carbon*, p 299, Plenum Press (1981).
6. Kennedy, I.M. "Models of soot formation and oxidation", *Progress in Energy and Comb. Science*, **23**, pp 95-132 (1997).

7. Toosi, R. "Surface analysis of combustion-generated soot particles by x-ray photoelectron spectroscopy", *Combustion and Flame*, **90**, pp 1-10 (1992).

8. Fulcheri, L. and Schwob, Y. "From methane to hydrogen, carbon black and water", *Int. J. Hydrogen Energy*, **20**(3), pp 197-202 (1995).

9. Jones, W.P. and McGuirk, J. "Computation of a round turbulent jet discharging into a confined cross flow", *Turbulent Shear Flows 2*, L.J.S. Bradbury et al., Ed., Springer, p 233 (1980).

10. Jones, W.P. and Whitelaw, J.H. "Calculation methods for reacting turbulent flows: A review", *Combustion and Flame*, **48**, pp 1-26 (1982).

11. Warnat, Z.J., Maas, U. and Dibbe, R.W. "Combustion", 3rd Ed., Springer-Verlag, Berlin, Germany (2001).

12. Tesner, P.A., Snegiriova, T.D. and Knorre, V.G. "Kinetics of dispersed carbon formation", *Combust. and Flame*, **17**, pp 253-260 (1971).

13. Tesner, P.A., Tsygankova, E.I., Guilazetdinov, L.P., Zuyev, V.P. and Loshakova, G.V. "The formation of soot from aromatic hydrocarbons in diffussion flames of hydrocarbon-hydrogen mixtures", *Combustion and Flame*, **17**, 279-285 (1971).

14. Magnussen, B.F. and Hjertager, B.H. "On mathematical models of turbulent combustion with special emphasis on soot formation and combustion", *16th Sym. (Int.) on Combustion*, The Combustion Institute, pp 719-729 (1976).

15. Murthy, J.Y. and Mathur, J. "A finite volume method for radiation heat transfer using unstructured meshes", *AIAA-98-0860* (Jan. 1998).

16. Smith, T.F., Shen, Z.F. and Friedman, "Evaluation of coefficients for the weighted sum of gray gases model", *J. Heat Transfer*, **104**, pp 602-608 (1982).

17. Sazhin, S.S. "An approximation for the absorption coefficient of soot in a radiating gas", *Manuscript. Fluent Europe*, Ltd (1994).

18. Ilbas, M. "Studies of ultra low NOx burners", PhD Thesis, University of Wales, UK (1997).

19. FLUENT 5.0.2, Fluent Incorporated, Lebanon, NH. (1998).

20. Sharif, M.A.R. and Wong, Y.K. "Evaluation of the performance of three turbulence closure models in the prediction of confined swirling flows", *Computers and Fluids*, **24**(1), pp 81-100 (1995).

21. Launder, B.E., Reece, G.J., and Rodi, W. "Progress in the development of a Reynolds-stress turbulence closure", *J. Fluid Mech.*, **68**(3), pp 537-566 (1975).

22. Launder, B.E. and Spalding, D.B. "The numerical computation of turbulent flows", *Computer Methods in Applied Mechanics and Engineering*, **3**, pp 269-289, (1974).